Environ Earth Sci (2013) 68:833–845
DOI 10.1007/s12665-012-1786-9

ORIGINAL ARTICLE

Analysis of the surface of different marbles by X-ray photoelectron spectroscopy (XPS) to evaluate decay by SO_2 attack

A. Luque · M. V. Martínez de Yuso · G. Cultrone · E. Sebastián

Received: 26 October 2011 / Accepted: 14 June 2012 / Published online: 3 July 2012

Abstract Atmospheric pollution is one of the main agents of decay in monuments and other works of art located in industrialised urban centres. SO_2 is a permanent and abundant component of air pollution and, although it does not have an immediate visual effect, after continuous exposure, it can cause irreversible damage to building materials. Marble is one of the most commonly used ornamental stones in historical monuments and its mineralogical composition makes it very susceptible to damage caused by exposure to SO_2. To measure the chemical reactions caused on marble by the action of atmosphere rich in SO_2, selected calcitic and dolomitic samples were altered by weathering accelerated test. For this, seven marble types (four calcitic and three dolomitic) were exposed to high concentration of sulphur dioxide for 24 h in a climate chamber under controlled temperature and humidity conditions (20 °C and $>$ 90 % HR). Changes on marble surfaces caused by reactions of SO_2 with calcite and dolomite were studied using two non-destructive techniques: chromatic change by means of colorimetry and chemical analysis using X-ray photoelectron spectroscopy (XPS). The development of new mineral phases was also observed by scanning electron microscopy. Colorimetric analysis revealed a decrease in lightness and chromatic parameters suggesting that these changes were due to the development of new mineral phases in all marbles. The XPS technique, which is generally used in the analysis of metals, is relatively new in the field of stone deterioration. It enabled us to recognise the development of sulphites and sulphates on marble surfaces with high precision, after just 24 h of exposure to high SO_2 concentrations and to distinguish different decay paths for calcitic and dolomitic marbles.

Keywords Marble decay · XPS · Calcium sulphite and sulphate · Magnesium sulphite and sulphate

A. Luque · G. Cultrone (✉) · E. Sebastián
Department of Mineralogy and Petrology, Faculty of Sciences, University of Granada, Avenida Fuentenueva s/n, 18002 Granada, Spain
e-mail: cultrone@ugr.es

A. Luque
e-mail: analuque@ugr.es

M. V. Martínez de Yuso
Central Research Services, University of Malaga, Bulevar Louis Pasteur, 33, Teatinos Campus, 29071 Malaga, Spain

Introduction

During the last century, the industrial process and the burning of coal in cities released increasing amounts of sulphur dioxide into the atmosphere, causing a severe pollution problem which became a subject of great concern in a variety of different scientific fields. Sulphur and nitrogen emissions are responsible for the formation of "acid rain" (or acid deposition), which influences climate change by modifying atmospheric and freshwater environments and damaging ecosystems and forests (Kellog et al. 1972; Tommervik et al. 1995; Seinfeld and Pandis 1998). Buildings, in general, and historical monuments, in particular, are also seriously affected by airborne pollution (Viles 1990; Török et al. 2011; Ghobadi and Momeni 2011).

Many researchers have focussed on gas emissions and have demonstrated that air pollution is a key factor in the decay of the materials used in the construction of our architectural heritage, which in many cases cause chromatic, chemical, biological and physical changes (Winkler

1966; Amoroso and Fassina 1983; Camuffo 1995; Antill and Viles 1999; Kontozova-Deutsch et al. 2011).

A large part of our architectural heritage is located in the centre of historic cities, areas in which there is a high concentration of motor vehicles and, in some cases, industries. Vehicles are the main source of aerosols enriched in C, S and N in the form of acids and, when they come into contact with construction materials (stone, brick, mortar, bronze, glass, etc.), start reacting on the surface (Fassina 1991; Rodríguez-Navarro and Sebastián 1996; Lefévre and Ausset 2002; Cultrone et al. 2008). The principal effect of this reaction is the formation and development of chemical weathering on the surface of the material, which enhances its decay and causes irreparable damage (Saiz-Jimenez et al. 2004).

The most frequently used construction and ornamental stones in historical monuments are carbonate based, because they were easily quarried and in abundant supply. They are however very sensitive to atmospheric pollution, especially sulphur dioxide. A great deal of research has been done on the effects of atmospheric pollution on old and new buildings made of limestones and/or calcarenites (Török 2002, 2008, Török et al. 2011; Luque et al. 2008a, b), dolostones (Olaru et al. 2010; López-Arce et al. 2008) and marbles (Feddema and Meierding 1987; Fassina et al. 2002; Lan et al. 2005). It has been demonstrated that the final effect of airborne SO_2 on carbonate materials is the development of sulphated black crusts on the stone surface (Brimblecombe 2004) and the loss of material due to solubilisation (López-Arce et al. 2008; Olaru et al. 2010).

Numerous researchers have investigated the mechanisms involved in the reaction and oxidation of SO_2 in calcitic carbonates (Böke et al. 2002; Gauri et al. 1973; Elfving et al. 1994) and, in many of them, it has been well established that calcium sulphite is the first stage in the process of calcium sulphate formation on the calcitic substrate. However, there are relatively few works that describe the initial chemical sulphation process on dolostones, and a full, detailed description of the reaction between SO_2 and dolomitic carbonates has so far not been provided (Gauri et al. 1992; López-Arce et al. 2009; Kulshreshtha et al. 1989).

According to Böke et al. (1999), the product formed by the reaction of SO_2 with calcareous stones under high relative humidity conditions is $CaSO_3{\cdot}1/2H_2O$ (calcium sulphite hemidrate) which, by oxidation of bisulphite ions, is transformed into $CaSO_4{\cdot}2H_2O$ (gypsum) as follows:

$$\begin{aligned} &CaCO_3\ (SO_2/H_2O) \rightarrow CaSO_3 \cdot 0.5H_2O \\ &CaSO_3 \cdot 1/2H_2O\ (O_2/H_2O) \rightarrow CaSO_4 \cdot 2H_2O \end{aligned} \quad (1)$$

On the contrary, when the sulphation process detailed above occurs on dolostones, it results in the formation of gypsum and epsomite as follows (Tambe et al. 1991):

$$CaMg(CO_3)_2 + 2SO_2 + 9H_2O + O_2 \rightarrow CaSO_4 \cdot 2H_2O + MgSO_4 \cdot 7H_2O + 2CO_2 \quad (2)$$

But, previous to the crystallisation of epsomite, an intermediate phase, i.e. magnesium sulphite, could have been developed. Magnesium sulphite and hydrates of magnesium sulphite are well-known salts in wet flue gas desulphurisation technology, and are used as reagents to absorb the SO_2 generated by coal-fired industrial processes or metal works (e.g. in wood, pulp and paper production) (Hagisawa 1993).

To this purpose, Przepiórski et al. (2012) noticed that $MgSO_3$ forms in porous carbon when SO_2 interacts with basic oxide anions on the surface of MgO particles, according to the reaction:

$$MgO + SO_2 \rightarrow MgSO_3 \quad (3)$$

Moreover, it is well described that the reaction of SO_2 from flue gases with an aqueous suspension of MgO results in the formation of $MgSO_3{\cdot}6H_2O$ or $MgSO_3{\cdot}3H_2O$ phases, depending on the prevailing conditions (Söhnel and Rieger 1994): below 40–42.5 °C magnesium sulphite hexahydrate is the stable equilibrium solid phase, while above this temperature the stable phase is the trihydrate (Pinaev 1964). However, due to the metastability of both phases, sulphur can react and form magnesium bisulphite, $Mg(HSO_3)_2$, making the desulphurisation process more difficult (Schöggl et al. 2006). Data on the solubility of magnesium sulphites are therefore of great importance, and previous researches have described how this solubility is directly related to the increase in magnesium sulphate content ($MgSO_4$) (Nývlt 2001).

In addition, the easy oxidation of $MgSO_3$ into $MgSO_4$ is a well-known effect (Rowland and Abdulsattar 1978; Liu et al. 2010). Hence, the same sulphation process that occurs on calcitic marbles can occur on dolomitic marbles as follow:

$$CaSO_3 \cdot 1/2H_2O + 1/2O_2 + 3/2\ H_2O \rightarrow CaSO_4 \cdot 2H_2O, \quad (4)$$

$$MgSO_3 + 1/2O_2 + 7H_2O \rightarrow MgSO_4 \cdot 7H_2O. \quad (5)$$

Przepiórski et al. (2012) noticed that the available literature does not contain appropriate X-ray diffraction patterns to confirm the presence of $MgSO_3$, while by means of X-ray photoelectron spectroscopy the presence of sulphur species (sulphite and y sulphate) was confirmed on the surface of porous carbon.

The aim of this paper is to identify the sulphated compounds that form on the surface of different types of marbles by using X-ray photoelectron spectroscopy. We also demonstrated that the mineralogical composition of marbles (calcitic and dolomitic) was the main factor that

influenced the formation rate of sulphite and sulphate species. To this end, Malaga-Starzec et al. (2004) observed that the stability of sulphites on the surface of calcite was twice as high as on the surface of dolomite, which is why the sulphation process had a more serious effect on calcitic marbles than on dolomitics. Finally, we found out if marble grain size and grain boundaries were other variables that played a role in sulphate development.

X-ray photoelectron spectroscopy (XPS) is a technique for surface analysis that provides information about the elemental and chemical composition of the uppermost atomic layers. In combination with low energy ion bombardment, which is used for depth profiling, this technique can be used for compositional and chemical analysis at different depths (Briggs and Seah 1983). In this case, secondary effects such as ion bombardment can induce chemical and compositional changes. As a consequence, only indirect information is obtained regarding the chemical and compositional state of the material being studied. From a technological point of view, ion bombardment can also be used for the modification of chemical and physical properties of surfaces, thus producing changes in the solid surface that can be exploited for certain applications of stone (Torrisi 2008) or metal (Santamarina et al. 2007) and even in research into nanoparticles (Kelly 1989; González-Elipe et al. 1993).

Materials used

We began by selecting seven marbles commonly used in Spain as construction and ornamental stones. Three of them (W*hite Macael*, *Tranco Macael* and *Yellow Macael*) came from quarries in the Sierra de los Filabres (Almeria), two (*Aroche* and *Fuenteheridos*) from the Sierra de Aracena (Huelva), one (W*hite Iberico*) from Sierra Tejeda (Granada), and the last (*White Mijas*) from Sierra Blanca (Malaga).

From a mineralogical point of view, all these marbles belong to either the calcitic, White Macael (WM), Tranco Macael (TM), Aroche (AR) and Fuenteheridos (FH), or the dolomitic, Yellow Macael (YM), White Iberico (WI) and White Mijas (MI) marble groups. However, within these groups, each marble has its own distinctive textural variations (Luque et al. 2011).

Methodology

Samples characterisation and experimental design

Mineralogical characterisation and petrographic features of the seven marbles prior to the sulphation test were determined by means of polarised optical microscopy (OM, Olympus BM-2).

To get a quick chemical reaction on marble surface, accelerated sulphation test was performed in a Kesternich chamber [details of the experimental setup are reported in Luque et al. (2008a, b)], at constant atmospheric pressure (1 atm), 25 °C, 90 % RH and 400 ppm SO_2 concentration for 24 h. A container full of water was introduced into the chamber to maintain high RH concentration. Marble samples were cut into two slabs of 10 × 10 × 0.3 cm and dried for 48 h at 50 °C before being placed in the chamber.

Colour variations

Before and after the sulphation test, colour measurements were carried out with a MINOLTA CR-210 colorimeter. Measurements were expressed using the CIE (Commission International de l'Eclairage) L^* a^* b^* system (Billmeyer and Salzman 1981), where L^* represents the lightness and a^* and b^* are the chromatic coordinates. The overall colour variation (ΔE) was evaluated using the following equation:

$$\Delta E = (\Delta L^{*2} + \Delta a^{*2} + \Delta b^{*2})^{1/2}.$$

Mineralogical determination

To identify the new phases developed on marbles surfaces, mineralogical analysis on unaltered and altered samples was performed by powder X-ray diffraction (XRD). We used a Philips PW-1710 diffractometer with graphite monochromator, automatic slit and CuKα radiation ($\lambda = 1.5405$ Å). Data were collected in step-scanning mode with 0.02° goniometer rate and 2θ from 3 to 60°. XRD goniometric calibration was performed using a silicon standard and the resulting data were interpreted using XPowder software (Martín 2004).

XPS analyses

In order to characterise the chemical phases developed on the surface of the seven marbles, X-ray photoelectron spectroscopy (XPS) analysis was performed; 4 keV Ar^+ bombardment was used to enable chemical analyses to be performed at greater depth. XPS spectra were recorded using a Physical Electronics PHI 5701 spectrometer with a multichannel hemispherical electroanalyser (SCAI, University of Malaga). Non-monochromatic MgKα X-ray (300 W, 15 kV, 1253.6 eV) was used as the excitation source. The spectrometer energy scale was calibrated using Cu 2*p*3/2, Ag 3*d*5/2 and Au 4*f*7/2 photoelectron lines at 932.7, 368.3 and 84.0 eV, respectively. The binding energy of photoelectron peaks was referenced to C 1*s* core level for adventitious carbon at 284.8 eV. High-resolution spectra were recorded at a given take-off angle of 45° by a concentric hemispherical analyser operating in the constant

pass energy mode at 29.35 eV and using a spot size 720 μm diameter aperture. The residual pressure in the analysis chamber was maintained below 1.33×10^{-7} Pa during the spectra acquisition. Marbles were mounted on a sample holder without adhesive tape and kept overnight under high vacuum in the preparation chamber before being transferred to the analysis chamber of the spectrometer for testing. Each spectral region was scanned in two areas with several sweeps until a good signal-to-noise ratio was observed. The PHI ACCESS ESCA-V8.0C software package was used for acquisition and data analysis. Recorded spectra were fitted using Gauss–Lorentz curves to determine the binding energy of the different element core levels more accurately (>90 %) (Briggs and Seah 1983). Atomic concentration percentages (A.C. %) of the characteristic marble elements were determined from high-resolution spectra after the subtraction of a Shirley-type background, and taking into account the corresponding area sensitivity factor for every photoelectron line (Moulder et al. 1992). Survey and multiregion spectra were recorded of C 1*s*, O 1*s*, Ca 2*p*, S 2*p* and Mg 2*p* photoelectron peaks.

A depth profiling study was carried out by 4 keV Ar^+ bombardment. The at-depth scale of 2.4 nm/min is assumed to be equivalent to the sputter rate of Ta_2O_5 under the same sputter conditions. Differences in sputtering yield between the sample being studied and Ta_2O_5 were not considered. Two depths were considered, after 2 min of Ar^+ bombardment (which corresponds to ~4.8 nm depth), and after 19 min of Ar^+ bombardment (~45.6 nm depth).

VPSEM observation

Visual observation of the marbles after the sulphation test was performed by means of a variable pressure scanning electron microscope (VPSEM) LEO 1430-VP, and the chemical composition of the crystals that developed on the surface was analysed with EDX microanalysis Inca 350 version 17 Oxford Instrument (CIC, University of Granada), which enables the identification of elements with low atomic numbers, including carbon.

Slab samples (10 × 10 × 3 cm) were dried for 48 h at 40 °C before being metalised with a mix of gold and platinum. The study was done in high vacuum at 20 kV and the images were acquired in a range from 10 to 20 kV.

Results and discussion

Samples characterisation

Table 1 summarises the petrological characteristics of the seven marbles.

Starting with the calcitic marbles, White Macael (WM) is characterised by a white pearl colour and a saccharoid texture. However, depending on the quarrying level, it may show a marked grey band with varying numbers of veins. Tranco Macael (TM) is a white marble with a heterogeneous grey banding and a smaller crystal size than WM. Aroche (AR) is a heterogeneous marble with extreme variability of grain size. It is saccharoid white in colour with some green/grey veins. Fuenteheridos (FH) differs from AR mainly in its smaller grain size and marked heterogeneous greenish banding.

As for the dolomitic marbles, Yellow Macael (YM), as its name suggests, is yellow and is characterised by its small grain size; White Iberico (WI) is a white marble with a marked grey band and small grain size; and White Mijas (MI) is a translucent white marble with the largest grain size of the dolomitic marbles.

Colour variations

Colour parameters were determined before and after exposure of the marbles to SO_2 and L^* a^* b^* values were plotted on two diagrams: the main chromatic changes were observed in a 2D diagram, while the lightness variations were better checked on a 3D diagram (Figs. 1, 2).

The YM sample appears separately from the other marbles (b^* is approximately 18) because of its distinctive yellow colour. The other samples fall near the origin of the axes (between −2 and 1 a^* values and 0 and 10 b^* values). The lightness (L^*) of all the marbles was very high, reaching values over 90.

After a weathering test (24 h of exposure to SO_2), significant variations could be observed in all samples. Chromatic values for all the marbles had shifted approximately one unit towards $-a^*$, while b^* remained almost unchanged. As for L^* values, all marbles showed a noticeable decrease (the average ΔL^* decrease was ~17.3) (Fig. 2). The marble that suffered the highest chromatic changes was YM (3.76) and the highest lightness change was AR (19.07), while the smallest chromatic changes were for FH (1.65) and the smallest lightness change was in WM (13.91).

The colour change undergone by all the samples ($\Delta E \geq 14$) denotes a significant alteration on the surface of all the marbles (Table 2), even if these changes are very small and are not visible to the naked eye.

Mineralogical determination

XRD analyses corroborated that there were no sulphate minerals on the surface of unaltered marbles. After 24 h of exposure to SO_2, all samples showed the presence of sulphates (Table 3). More in detail, calcium sulphite hydrate

Table 1 Petrological features of the studied marbles

	Main mineralogical composition	Texture	Grain boundary	Grain size
WM	Calcitic	Granoblastic	Straight	0.1–3
TM	Calcitic	Granoblastic	Lobate	0.2–1.5
AR	Calcitic	Porphyroblastic	Amoeboid	0.4–1
FH	Calcitic	Granoblastic	Straight	0.1–0.4
YM	Dolomitic	Granoblastic	Straight and lobate	0.02–1
WI	Dolomitic	Porphyroblastic	Lobate	0.1–0.4
MI	Dolomitic	Granoblastic	Amoeboid	0.1–4

WM White Macael, *TM* Tranco Macael, *AR* Aroche, *FH* Fuenteheridos, *YM* Yellow Macael, *WI* White Iberico, *MI* White Mijas

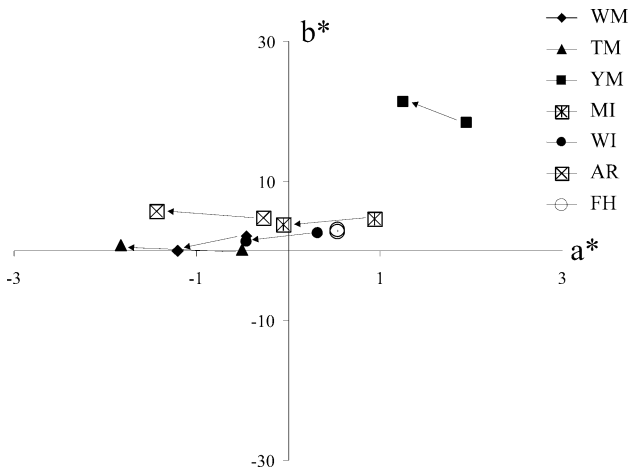

Fig. 1 Chromatic parameters (a^* and b^*) for unaltered and altered marbles (*the arrow* indicates the change from unaltered to altered samples). *WM* White Macael, *TM* Tranco Macael, *AR* Aroche, *FH* Fuenteheridos, *YM* Yellow Macael, *WI* White Iberico, *MI* White Mijas

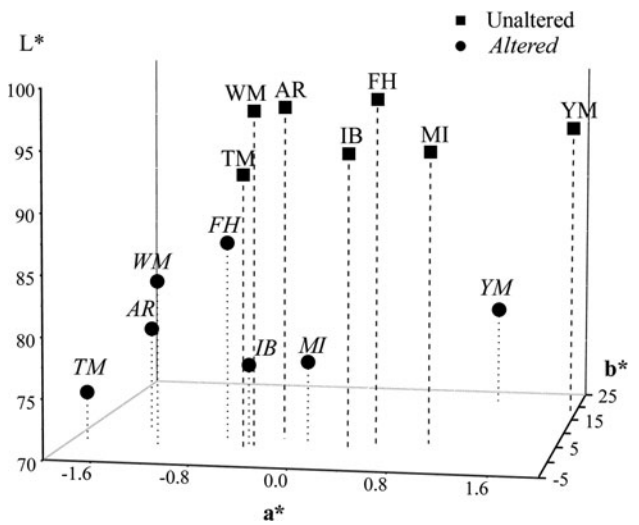

Fig. 2 CIE L^* a^* b^* parameters for unaltered (*square*) and altered (*circle*) marbles: chromaticity (a^* and b^*) versus lightness (L^*). *WM* White Macael, *TM* Tranco Macael, *AR* Aroche, *FH* Fuenteheridos, *YM* Yellow Macael, *WI* White Iberico, *MI* White Mijas

($CaSO_3 \cdot H_2O$) was the most common new phase and formed in all marbles. Lesser amounts of gypsum ($CaSO_4 \cdot 2H_2O$) were identified in WM, WI and MI samples, while only on two dolomitic marbles surfaces, YM and WI, hexahydrite ($MgSO_4 \cdot 6H_2O$) was found.

XPS analyses

A first survey spectra recorded in each marble surface showed that the main chemical elements present on unaltered marble were C, O, Ca and Mg, while on altered marbles C, O, Ca, Mg and S were present.

The high-resolution spectra of selected peaks allowed us to determine their different contributions in terms of the atomic concentration percentage (A.C. %) of C 1*s*, O 1*s*, Ca $2p_{3/2}$, Mg $2p_{3/2}$ and S $2p_{3/2}$. From the binding energy and intensity of each photoelectron peak, the elemental identity and chemical state of these elements can be determined (Briggs and Grant 2003).

A detailed study of the photoelectron peak S 2*p* signal recorder in both marble groups can determine the contribution that identifies the different sulphur compounds developed on calcitic and dolomitic marbles surfaces after their exposure to SO_2.

High-resolution spectra of selected peaks

From high-resolution spectra, we measured the atomic concentration percentage (A.C. %) of selected peaks of C, O, Ca, Mg and S, detected on the surface of unaltered and at a depth of ~45.6 nm of altered marbles (Table 4).

The A.C. percentages of C, O, Ca and Mg values fit quite well with the mineralogical (calcitic and dolomitic) composition of unaltered marbles. In addition, the low S value measured in all samples (<1 %) confirmed that sulphur compounds were not present on marble surfaces (Table 4) after argon ion bombardment.

When altered calcitic and dolomitic marbles were analysed on the surface and at depth (after 19 min of argon ion bombardment), XPS analyses showed a different trend.

Table 2 Overall colour change (ΔE) in marbles after sulphation test

	Calcitic				Dolomitic		
	WM	*TM*	*AR*	*FH*	*YM*	*WI*	*MI*
ΔE	14.08	18.46	19.13	17.51	17.03	17.57	17.63

WM White Macael, *TM* Tranco Macael, *AR* Aroche, *FH* Fuenteheridos, *YM* Yellow Macael, *WI* White Iberico, *MI* White Mijas

Table 3 Mineralogical phases detected on marbles surface by XRD after SO_2 exposition

	Calcium sulphite hydrate ($CaSO_4 \cdot H_2O$)	Gypsum ($CaSO_4 \cdot 2H_2O$)	Magnesium sulphate hexahydrate ($MgSO_4 \cdot 6H_2O$)
Calcitic			
WM	X	X	
TM	X		
AR	X		
FH	X		
Dolomitic			
YM	X		X
WI	X	X	X
MI	X	X	

WM White Macael, *TM* Tranco Macael, *AR* Aroche, *FH* Fuenteheridos, *YM* Yellow Macael, *WI* White Iberico, *MI* White Mijas

Table 5 shows different chemical compounds with their binding energies determined by the chemical state of C, O, Ca, Mg and S.

Calcitic marbles Surface analysis of altered marbles showed that the values of S content (~16 %) measured in all samples was approximately three times higher than the C (as carbonate) content (~6 %), while Ca plus Mg values (~15 %) versus S content were constant. When analyses were carried out at depth (~45.6 nm), the S content (~9.5 %) decreased significantly with respect to C content (~4 %) and the sum of Ca and Mg content (~25 %) was now approximately twice the S content (Table 4).

Dolomitic marbles Surface analysis showed that the values of the S content (~6 %) was approximately half the C content (14 %) and the sum of the Ca and Mg values (~19 %) was clearly twice that of the S content. At a greater depth (~45.6 nm), the S content fell by half (~3 %), C slightly decreased (~10 %) and the Ca plus Mg content (~28 %) increased noticeably up to 20 times higher than the S content (Table 4).

This analysis shows that the sulphur content (S %) measured in both marble groups is higher in all calcitic marbles than in dolomitics, regardless of their grain size and boundaries.

High-resolution spectra of S 2p on marbles

The interpretation (curve shape and binding energy) of high-resolution spectra of the photoelectron peak S 2*p* signal recorder in all marbles allowed us to identify the different contributions of sulphur compounds present on calcitic and dolomitic surfaces.

Deconvoluted spectra were adjusted with an average value of the peak width at half height (FWHM) at 1.75 eV value for MgKα radiation and the average Gauss peak-shape of 90.

After the subtraction of Shirley background, the data were fitted with model lines corresponding to two chemical species. Each chemical species was modelled with a spin–orbit doublet and the shift between S $2p_{3/2}$ and S $2p_{1/2}$ components was set on 1.18 eV and intensity ratio was 2:1 (Moulder et al. 1992).

Regarding the curve shape, we can mention that all S 2*p* spectra recorder on the surface of calcitic and dolomitic marbles were similar for each marble group even when these analyses were carried out at depth.

S $2p_{3/2}$ spectra obtained on calcitic marbles showed their maximum binding energy at 166.7 eV and asymmetrical shape to higher values (~168.7 eV), suggesting that two contributions can be deconvoluted in this region. However, the same spectra collected in dolomitic marbles, more irregular and wider than that in calcitic marbles, suggests that more contributions can be deconvoluted in this region.

Regarding the S $2p_{3/2}$ core level spectra obtained in seven marbles after 19 min (~45.6 nm depth) of Ar^+ bombardment, another photoemission at a binding energy of 161.5 eV is attributed to reduced sulphur compounds.

Calcitic marbles The S 2*p* spectra obtained on the surface and after 19 min (~45.6 nm depth) of Ar^+ bombardment were deconvoluted into two contributions (Figs. 3, 4): $CaSO_3$ (166.8 ± 0.1 eV) and $CaSO_4$ (168.8 ± 0.2 eV). The measurement of $CaSO_3$ (sulphite) and $CaSO_4$ (sulphate) photoemissions from the photoelectron peak S 2*p* allowed us to determine their contents (in %) from different layers (on surface and at depth).

In general, the values of sulphites obtained on calcitic marbles are always higher than values of sulphates on surface and at depth, although for both sulphur compounds

Table 4 Atomic concentration of O, Ca, Mg, and S elements relative to C concentration (in %) calculated for seven unaltered and altered marbles (on the surface and after 19 min of sputtering)

	C (%)	*	O (%)	*	Ca (%)	*	Mg (%)	*	S (%)	*
Fresh marbles										
Surface										
Calcitic										
WM	23.47	13,115	60.60	84,748	14.97	52,243	0.60	167	0.36	444
TR	19.78	17,951	60.80	138,138	19.20	108,833	0.08	37	0.14	284
AR	20.76	12,110	62.30	90,970	15.78	57,488	0.81	237	0.35	445
FH	20.40	19,308	60.03	142,196	19.03	112,436	0.41	193	0.14	292
Dolomitic										
YM	19.16	14,996	59.65	116,831	11.22	54,803	9.49	3,713	0.48	832
WI	19.48	9,546	60.51	74,201	9.68	29,595	9.67	2,367	0.66	718
MI	19.98	14,485	59.97	108,838	10.59	47,943	8.60	3,117	0.87	1,393
Altered marbles										
Surface										
Calcitic										
WM	8.45	5,024	61.74	9,183	11.37	42,174	3.58	19,517	14.86	1,064
TR	5.03	5,222	61.52	159,790	13.57	87,948	2.42	40,034	17.45	1,255
AR	4.52	5,020	65.99	183,568	13.35	92,638	0.92	513	15.22	37,394
FH	5.09	5,528	61.54	167,370	12.34	83,750	5.08	2,760	15.95	38,317
Dolomitic										
YM	13.01	10,900	61.22	128,394	6.66	34,850	12.74	5,338	6.37	11,802
WI	15.26	23,009	61.87	233,567	9.85	92,711	9.87	7,442	3.16	10,527
MI	14.07	12,426	59.42	131,320	5.96	32,872	10.82	4,790	9.70	18,925
After 19 min										
Calcitic										
WM	8.60	11,884	56.03	193,776	24.01	207,138	0.75	515	10.61	32,401
TR	2.59	4,094	62.40	247,266	26.24	259,350	0.37	292	8.40	29,409
AR	2.77	4,074	64.97	239,382	23.25	213,710	0.48	351	8.53	27,764
FH	3.20	5,080	60.23	239,156	23.10	228,808	2.89	2,290	10.59	37,132
Dolomitic										
YM	9.66	16,412	59.04	263,908	15.63	176,912	12.88	11,530	2.78	11,256
WI	11.99	31,274	61.02	405,764	13.61	225,306	12.08	16,061	1.35	7,906
MI	8.15	14,100	58.01	251,286	13.75	148,564	13.55	11,721	6.54	25,030

WM White Macael, *TM* Tranco Macael, *AR* Aroche, *FH* Fuenteheridos, *YM* Yellow Macael, *WI* White Iberico, *MI* White Mijas

* Area: Absolute intensity in cts-eV/s

values decrease with depth (Table 6). On the surface, $CaSO_3$ contents (~83 %) are four times higher than the $CaSO_4$ values (~17 %), while at depth a strong decrease in calcium sulphite content (~53 %) and a slight increase in calcium sulphate content (~34 %) can be observed.

As one can see, low values of reduced sulphur contents were detected (binding energy at 161.1 eV) when calcitic marbles were analysed at depth (Table 6).

Dolomitic marbles In these marbles, the S 2*p* spectra obtained on the surface and after 19 min (~45.6 nm depth) of Ar^+ bombardment were deconvoluted into four contributions (Figs. 5, 6): $CaSO_3$ (166.8 ± 0.1 eV), $MgSO_3$ (167.4 ± 0.2 eV), $CaSO_4$ (168.8 ± 0.2 eV) and $MgSO_4$ (169.4 ± 0.3 eV).

With the exception of YM and similarly to calcitic marbles, values of sulphites ($CaSO_3$ and $MgSO_3$) detected on surface and at depth were higher than those of sulphates ($CaSO_4$ and $MgSO_4$). Nevertheless, some differences can be noticed when values of calcium (Ca-sulphite and sulphate) and magnesium species (Mg-sulphite and sulphate) are compared on surface and at depth (Table 7).

Surface analysis showed that calcium species concentrations (>46 %) measured in dolomitic marbles were slightly higher than magnesium species concentrations (<44 %). When analysis was carried out at depth (~45.6 nm), the

Table 5 Binding energy (in eV) of *O* Oxygen, *C* Carbon, *Ca* Calcium, *Mg* Magnesium and *S* Sulphur peaks for different oxidation states of chemical compounds

Element	Compound	BE (eV)	Element	Compound	BE (eV)	Literature references (eV)
C 1*s*	$CaCO_3$/Ca, $Mg(CO_3)_2$	289.2	S 2*p*	$CaSO_3$	166.8	166.9; Siriwardene et al. (1986)
O 1*s*	CaC_3//Ca, $Mg(CO_3)_2$	531.2				166.7; Lindberg et al. (1970)
	$CaSO_3$	531.9				167.0; Baltrusaitis et al. (2007)
	$CaSO_4$	532		$MgSO_3$	167.4	167.5; Przepiórski et al. (2012)
	$MgSO_4$	531.7				167.0; Craig et al. (1974)
Ca 2*p*	$CaCO_3$/Ca, $Mg(CO_3)_2$	346.6		$CaSO_4$	168.8	169.0; Christie et al. (1983)
	$CaSO_3$	346.5				169.0; Moulder et al. (1992)
	$CaSO_4$	348				168.9; Lindberg et al. (1970)
Mg 2*p*	$CaCO_3$/Ca, $Mg(CO_3)_2$	48.6		$MgSO_4$	169.4	169.7; Przepiórski et al. (2012)
	$MgSO_4$	51.4				169.7; Craig et al. (1974)

Literature data for these compounds is indicated

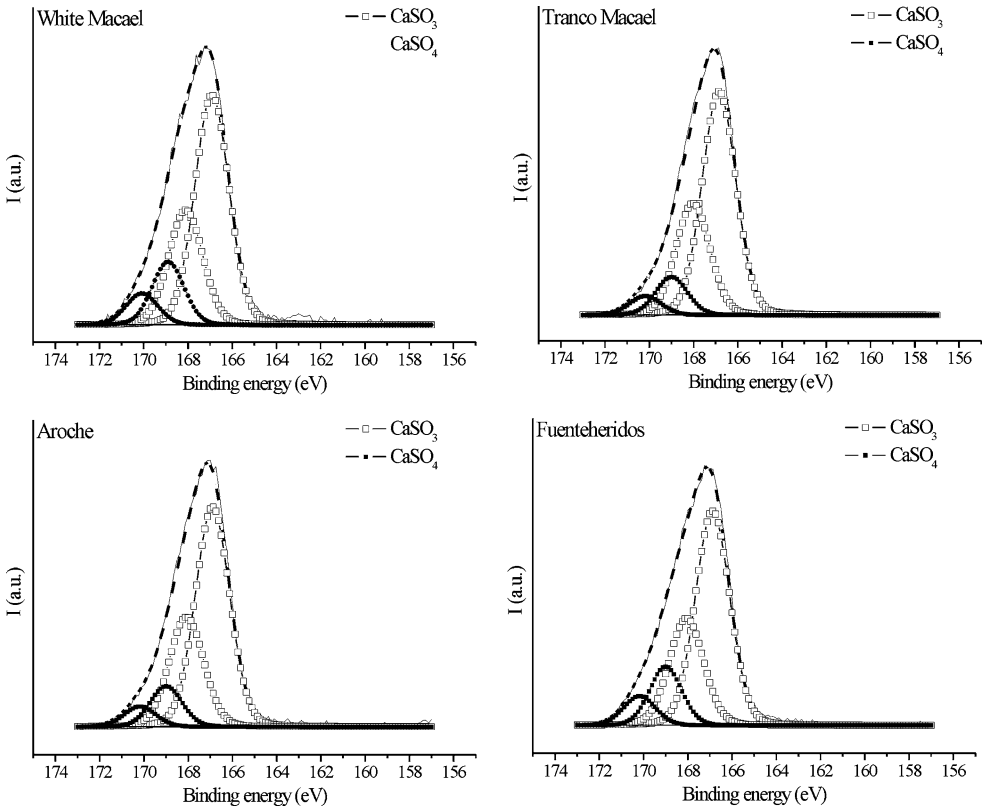

Fig. 3 S 2*p* core level spectra region (*dashed lines*) deconvoluted into each contribution ($CaSO_3$ and $CaSO_4$) on the surface of calcitic marbles. Binding energy (eV) versus intensity (a.u.)

calcium species concentrations (<39 %) decreased significantly with respect to magnesium species concentrations (>51 %) which even showed a slight increase.

Likewise to calcitic marbles, low values of reduced sulphur contents were detected (binding energy at 161.4 eV) when dolomitic marbles were analysed at depth (Table 6). However, considering that this phase was not detected on surface analysis, its presence can be attributed to sputtering processes. Moreover, considering that in dolomitic marbles, $MgSO_3$ concentrations slightly increased in depth, reduced sulphur can only be due to a reduction of sulphites. Ion bombardment in metal sulphates has evidenced a partial susceptibility to damage of hydrated calcium sulphate from radiation, whereas $CaSO_4$ proved to be more resistant (Coyle et al. 1981).

Reduction of oxides during ion bombardment is known and numerous research have related how the oxide ion is reduced preferably during analyses sputtering (Briggs and Seah 1983). According to Christie et al. (1981), the oxygen photoelectron peak having the lower binding energy may

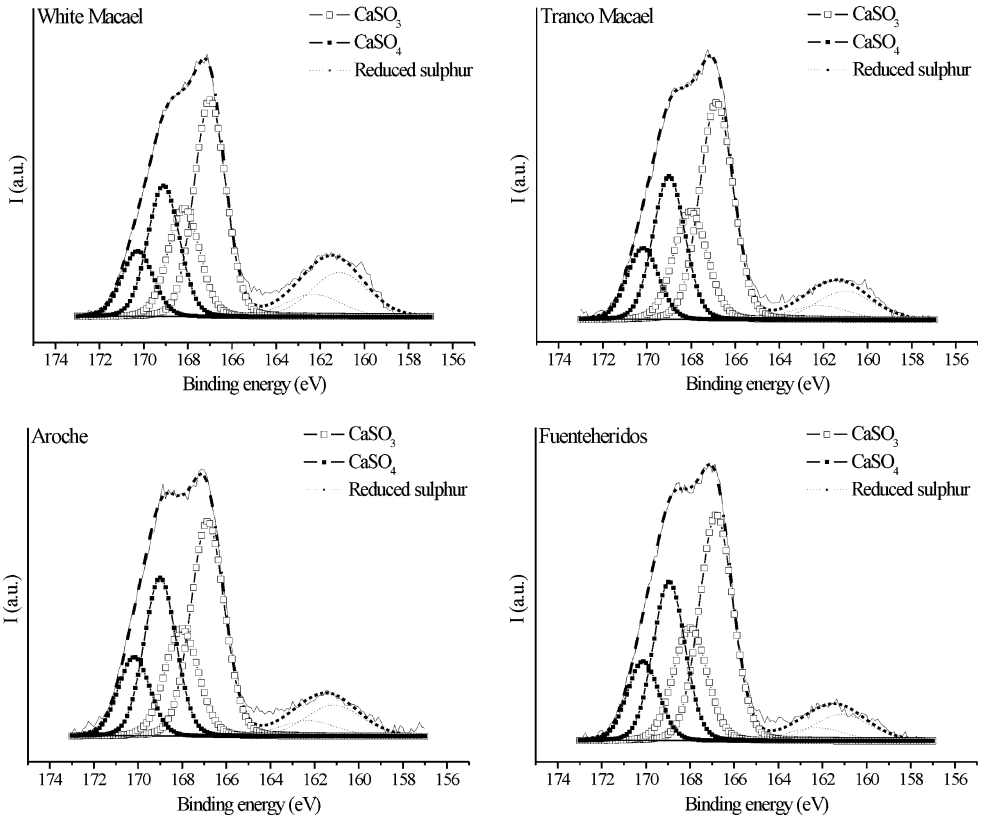

Fig. 4 S 2*p* core level spectra region (*dashed lines*) deconvoluted into each contribution ($CaSO_3$ and $CaSO_4$) in-depth (~ 45.6 nm) of calcitic marbles. Binding energy (eV) versus intensity (a.u.). The component corresponding to reduced sulphur (*dotted lines*) is clearly evident after the ion bombardment

Table 6 Calcium sulphite, calcium sulphate, and reduced sulphur content in calcitic marbles on the surface and after 19 min of sputtering (45.6 nm) Ar^+ bombardment

	Calcium sulphate (%)	Calcium sulphite (%)	Reduced sulphur
Surface			
WM	20.4	79.6	0
TR	13.9	86.1	0
AR	14.7	85.3	0
FH	20.3	79.7	0
After 19 min			
WM	30.8	50.8	18.4
TR	33.9	54.2	11.9
AR	36.0	51.6	12.4
FH	35.7	53.8	10.5

WM White Macael, *TM* Tranco Macael, *AR* Aroche, *FH* Fuenteheridos

be assigned to the oxide formed as a result of ion bombardment, and the intensity of the peak is thus a measure of the extent of decomposition.

VPSEM observations

VPSEM images corroborate the sulphation process in marble surfaces after a very short period (24 h) of exposure to SO_2. The morphology and the size of the new sulphate phases can also be identified. Calcitic marbles show the biggest crystal size of the sulphated products scattered on the surface of the sample (see White Macael and Tranco Macael, Fig. 7a and b), whereas dolomitic marbles have few crystallised areas but have a high concentration of small crystals of sulphated products (see White Iberico and White Mijas, Fig. 7c and d).

Finally, the main difference between the calcitic (WM and TM) and the dolomitic marbles (WI and MI) is in the morphology of the new crystals that develop. In calcitic marbles the crystals are like tabular aggregates, whereas in dolomitic marbles two different morphologies can be observed: rosette and tabular crystals in WI and a radiating cluster of needle-like crystals in MI.

Conclusions

In this work, we have demonstrated that the surfaces of calcitic and dolomitic marbles suffer chemical attack after just 24 h of exposure to SO_2, The combined techniques used in this research have identified and confirmed early stages of sulphation on the surface of the marbles.

Air pollution is a decay factor that produces several colour changes in the stone surface, even with minimal exposure to air pollution. The chromatic parameters and,

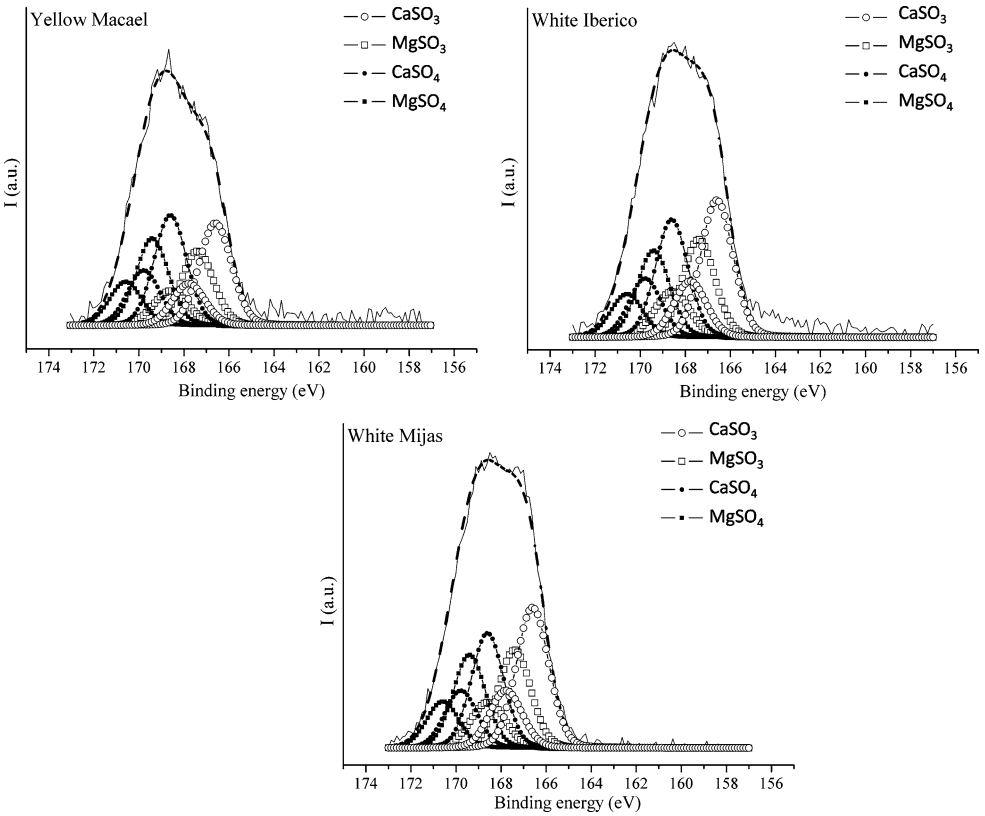

Fig. 5 S 2*p* core level spectra region (*dashed lines*) deconvoluted into each contribution ($CaSO_3$, $CaSO_4$, $MgSO_3$, and $MgSO_4$) on the surface of dolomitic marbles. Binding energy (eV) versus intensity (a.u.)

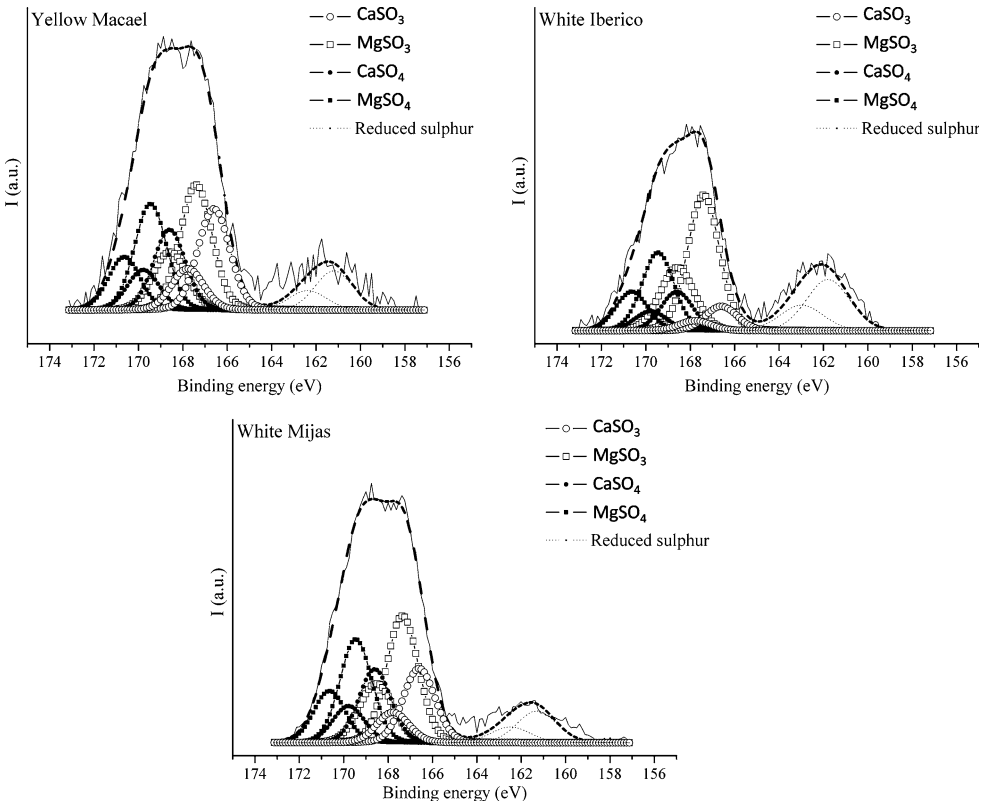

Fig. 6 S 2*p* core level spectra region (*dashed lines*) deconvoluted into each contribution ($CaSO_3$, $CaSO_4$, $MgSO_3$, and $MgSO_4$) at depth (~45.6 nm) for dolomitic marbles. Binding energy (eV) versus intensity (a.u.). The component corresponding to reduced sulphur (*dotted lines*) is clearly apparent after the ion bombardment

Table 7 Magnesium and calcium sulphate, magnesium and calcium sulphite and reduced sulphur content in dolomitic marbles on the surface and after 19 min sputtering (45.6 nm) Ar^+ bombardment

	Magnesium sulphate (%)	Calcium sulphate (%)	Magnesiun sulphite (%)	Calcium sulphite (%)	Reduced sulphur
Surface					
YM	23.7	30.0	20.2	26.1	0
WI	20.1	26.5	21.6	31.8	0
MI	20.3	26.2	22.4	31.1	0
After 19 min					
YM	23.4	17.7	27.6	21.0	10.2
WI	22.6	11.3	39.3	6.6	20.1
MI	25.1	17.8	30.7	16.9	9.5

YM Yellow Macael, *WI* White Iberico, *MI* White Mijas

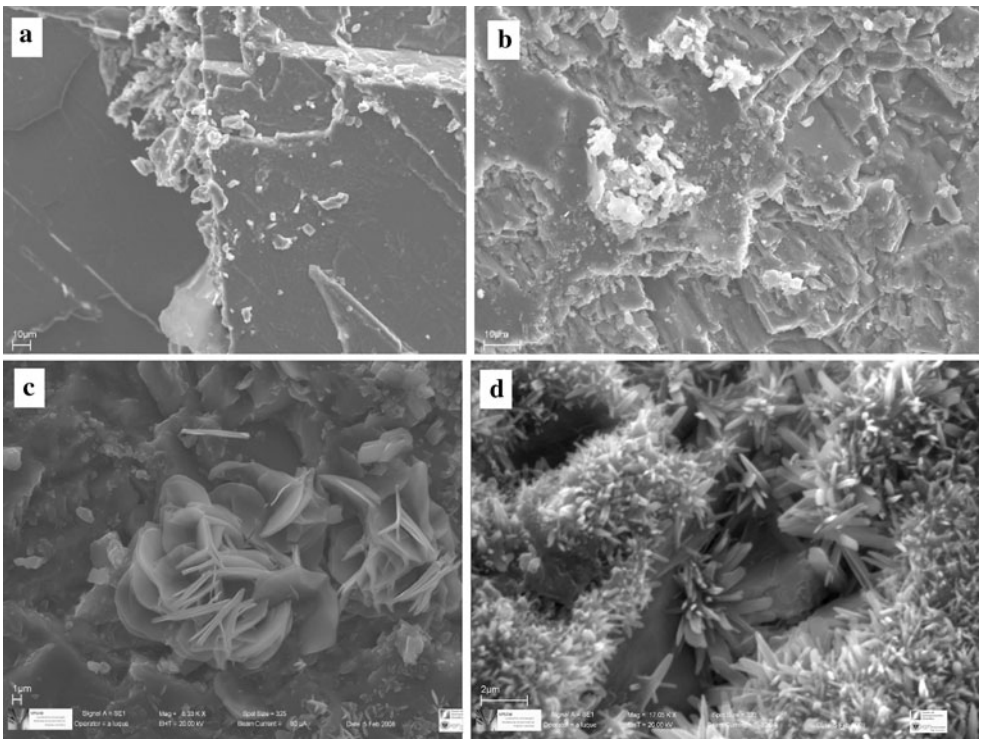

Fig. 7 Microphotographs showing the development of different crystal shapes on the surfaces of four marbles (**a** White Macael, **b** Aroche, **c** White Iberico and **d** White Mijas) at the end of the sulphation test

above all, the lightness measured before and after exposure to SO_2 suggest that some chemical processes have occurred on the surface of the marbles.

Only $CaSO_3$, $CaSO_4$ and $MgSO_3$ phases were detected by XRD, while XPS analyses showed great accuracy in the identification and quantification of calcium and magnesium sulphite and sulphate phases formed on the seven marbles. These phases were then observed under scanning electron microscopy (VPSEM) showing the different morphologies, sizes and the population density of the new minerals that developed.

We have noticed that calcitic marbles show higher rates of sulphation than dolomitic marbles, and also that in all marbles (calcitic and dolomitic), sulphite concentrations are always higher than sulphate concentrations. According to Malaga-Starzec et al. (2004), this is due to the stability of sulphite on calcite which is twice as high as on dolomite.

The sulphation process in calcitic marbles begins with the development of calcium sulphite which is then transformed by oxidation into calcium sulphate. As we have seen on the surface and at 45.6 nm depth, this reaction occurs early and at shallow depth. However, when sulphation process occurs in dolomitic marbles, although it begins with the development of calcium and magnesium sulphite, the subsequent transformations into calcium and magnesium sulphate are not clear.

Surface analysis by XPS shows that calcium sulphite and sulphate concentrations are higher than magnesium sulphite and sulphate. When XPS is carried out at depth, calcium sulphite and sulphate concentrations show a slight decrease compared to magnesium sulphite and sulphate. In addition to these phases, reduced sulphur was also detected after ion bombardment of calcitic and dolomitic marbles. Coyle et al. (1981) suggested that the development of reduced sulphur was due to the sensitivity of hydrated calcium sulphite to sputtering processes. Conversely, Christie et al. (1983) have not evidenced this phenomenon. Therefore, we consider that further analyses must be carried out to better explain the sensitivity of calcium sulphite to ion bombardment process.

In addition, although the sulphation processes affecting calcitic materials have been well described in literature, this is not the case for dolomitic materials, in which the development of magnesium sulphite has not been identified so far. Even if magnesium sulphite was not detected by X-ray diffraction, the excess Mg atomic concentration with respect to Ca atomic concentration (see Table 4) was not comparable to the rates of magnesium and calcium sulphate formation, which led us to think that part of this magnesium can be present as magnesium sulphite (Przepiórski et al. 2012).

The absence of magnesium sulphite in marbles damaged by exposure to SO_2 may be caused by both, the higher solubility of $MgSO_3$ in the presence of $MgSO_4$ (Nývlt 2001) and the early oxidation of $MgSO_3$ to $MgSO_4$, thus preventing the formation of magnesium sulphite (Rowland and Abdulsattar 1978; Liu et al. 2010). The absence of sulphite may even explain why less magnesium sulphates (epsomite) develop on dolomite substrates than calcium sulphates (gypsum).

It is evident that the mineralogical composition of marbles is the main factor influencing the formation of sulphites and sulphates on the surface, while the grain size and grain boundaries do not have much influence on these reactions. We have observed that the sulphation trend is the same for all calcitic and dolomitic marbles, regardless of their particular fabric.

Our research confirms that XPS is a great tool to help us understand the different chemical processes that occur in stone surfaces after a very short period of exposure to air pollution, because it is able to detect the development of decay crusts measuring only a few micrometres.

Acknowledgments This research was financed by Research Projects P09-RNM-4905 and FQM 1635 and the Research Group RNM-179 (Junta de Andalucía, Spain). We thank E. Ruiz-Agudo and C. Rodriguez-Navarro for their assistance in the interpretation of chemical analyses and Nigel Walkington for the translation of the manuscript.

References

Amoroso GG, Fassina V (1983) Stone decay and conservation. Elsevier, Amsterdam

Antill SJ, Viles HA (1999) Aspects of stone weathering, decay and conservation. Imperial College Press, London, pp 28–42

Baltrusaitis J, Usher CR, Grassian VH (2007) Reactions of sulfur dioxide on calcium carbonate single crystal and particle surfaces at the adsorbed water carbonate interface. Phys Chem Chem Phys 9:3011–3024

Billmeyer FW, Salzmanm M (1981) Principles of color technology, 2nd edn. Wiley, New York

Böke H, Göktürk H, Caner-Saltık E, Demirci S (1999) Effect of airborne particle on SO_2–calcite reaction. Appl Surf Sci 140:70–82

Böke H, Hale-Göktürk EH, Caner-Saltık E (2002) Effect of some surfactants on SO_2–marble reaction. Mater Lett 57:935–939

Briggs D, Seah MP (1983) Practical surface analysis by Auger and X-ray photoelectron spectroscopy. In: Briggs D, Seah MP (eds) Wiley, Chichester

Briggs D, Grant JT (2003) Surface analysis and X-ray photoelectron spectroscopy. IM Publications, Chichester

Brimblecombe P (2004) Air pollution and cultural heritage. In: Saiz-Jimenez C (ed) London, pp 87–90

Camuffo D (1995) Physical weathering of stones. Sci Total Environ 167(1–3):1–14

Christie AB, Sutherland I, Walls JM (1981) An XPS study of ion-induced dissociation on metal carbonate surfaces. Vaccum 31:513–517

Christie AB, Lee J, Sutherland I, Walls JM (1983) An XPS study of ion-induced compositional changes with group II and group IV compounds. Appl Surf Sci 15:224–237

Coyle GJ, Tsang T, Adler I, Ben-Zvi N (1981) XPS studies of ion-bombardment damage of transition metal sulfates. J Electron Spectrosc Relat Phenom 24:221–236

Craig NL, Harker AB, Novakov T (1974) Determination of the chemical states of sulfur in ambient pollution aerosols by X-ray photoelectron spectroscopy. Atmos Environ 8:15–21

Cultrone G, Arizzi A, Sebastián E, Rodríguez-Navarro C (2008) Sulfation of calcitic and dolomitic lime mortars in the presence of diesel particulate matter. Environ Geol 56:741–752

Elfving P, Panas I, Lindqvist O (1994) Model study of the first steps in deterioration of calcareous stone. Initial surface sulphite formation on calcite. Appl Surf Sci 74:91–98

Fassina V (1991) Atmospheric pollutants responsible for stone decay. Wet and dry surface deposition of air pollutants on stone and the formation of black scabs. In: Zezza F (ed) Weathering and air pollution. Community of Mediterranean Universities, Bari, pp 67–86

Fassina V, Favaro M, Naccari A (2002) Principal decay patterns on venetian monuments. In: Siegesmund S, Weiss TS, Vollbrecht A (eds) Natural stones, weathering phenomena, conservation strategies and case studies, special publications 205. Geological Society, London, pp 381–391

Feddema JJ, Meierding TC (1987) Marble weathering and air pollution in Philadelphia. Atmos Environ 21(1):143–157

Gauri KL, Doderer GC, Lipscomb NT, Sarma AC (1973) Reactivity of treated and untreated marble specimens in an SO_2 atmosphere. Stud Conserv 18:25–35

Gauri KL, Tambe SS, Caner-Saltık EN (1992) Weathering of dolomite in industrial environments. Environ Geol Water Sci 19:55–63

Ghobadi MH, Momeni AA (2011) Assessment of granitic degradability susceptive to acid solutions in urban area. Environ Earth Sci 64:753–760

González-Elipe AR, Fernández A, Caballero A, Holgado JP, Munuera G (1993) Mixing effects in CeO_2/TiO_2 and CeO_2/SiO_2 systems submitted to Ar^+ sputtering. J Vac Sci Technol A 11:58–65

Hagisawa H (1933) Studies of magnesium sulphite. Bull Inst Phys Chem Res 12:976–983

Kellogg WW, Cadle RD, Allen ER, Lazrus AL, Martell EA (1972) The sulfur cycle. Science 175(22):587–596

Kelly R (1989) Bombardment-induced compositional change with alloys, oxides, oxysalts and halides III. The role of chemical driving forces. Mater Sci Eng 115:11–24

Kontozova-Deutsch V, Cardell C, Urosevic M, Ruiz-Agudo E, Deutsch F, Van Grieken R (2011) Characterization of indoor and outdoor atmospheric pollutants impacting architectural monuments: the case of San Jerónimo Monastery (Granada, Spain). Environ Earth Sci 63:1433–1445

Kulshreshtha NP, Punuru AR, Gauri KL (1989) Kinetics of the reaction of SO_2 with marble. J Mater Civil Eng 1:60–72

Lan TTN, Nishimura R, Tsujino Y, Satoh Y, Thoa NTP, Yokoi M, Maeda Y (2005) The effects of air pollution and climatic factors on atmospheric corrosion of marble under field exposure. Corros Sci 47:1023–1038

Lefévre RA, Ausset P (2002) Atmospheric pollution and building materials: stone and glass. In: Siegesmund S, Weiss T, Vollbrecht A (eds) Natural stone, weathering phenomena, conservation strategies and case studies. Special Publications, vol 205. Geological Society, London, pp 329–345

Lindberg BJ, Hamrin K, Johansson G, Gelius U, Fahlman A, Nordling C, Siegbahn K (1970) Molecular spectroscopy by means of ESCA II. Sulfur compounds. Correlation of electron binding energy with structure. Physica Scryta 1:286–287

Liu Y, Bisson TM, Yang H, Xu Z (2010) Recent developments in novel sorbents for flue gas clean up. Fuel Process Technol 91:1175–1197

López-Arce P, Doehne E, Martin W, Pinchin S (2008) Sales de sulfato magnésico y materiales de edificios históricos: simulación experimental de laminaciones en calizas mediante ciclos de humedad relativa y cristalización de sales. Materiales de Construcción 58(289–290):125–142

López-Arce P, García-Guinea J, Benavente D, Tormo L, Doehne E (2009) Deterioration of dolostone by magnesium sulphate salt: an example of incompatible building materials at Bonaval Monastery. Constr Build Mater 23(2):846–855

Luque A, Cultrone C, Sebastián E, Cazalla O (2008) Evaluación de la eficacia de tratamientos en el incremento de la durabilidad de una calcarenita bioclástica (Granada, España), vol 58(292), pp 115–128

Luque A, Sebastián EM, Cultrone G, Ruiz-Agudo E (2008) Análisis mediante XPS para la determinación de yeso neoformado por contaminación mediante SO_2. In: Proceedings of 9th international congress on heritage and building conservation, Seville, pp 75–80

Luque A, Leiss B, Álvarez-Lloret P, Cultrone G, Siegesmund S, Sebastián E, Cardell C (2011) Potential thermal expansion of calcitic and dolomitic marbles from Andalusia (Spain). J Appl Crystallogr 44:1227–1237

Malaga-Starzec K, Panas I, Lindqvist O (2004) Model study of initial adsorption of SO_2 on calcite and dolomite. Appl Surf Sci 222:82–88

Martín JD (2004) A software package for powder X-ray diffraction analysis. Lgl. Dep. GR 1001/04

Moulder JF, Stickle WF, Sobol PE, Bomben KD (1992) Handbook of X-Ray photoelectron spectroscopy. In: Chastain J (ed) Perkin-Elmer Corporation, Minneapolis, pp 72

Nývlt J (2001) Solubilities of magnesium sulphite. J Therm Anal Calorim 66:509–512

Olaru M, Aflori M, Simionescu B, Doroftei F, Stratulat L (2010) Effect of SO_2 dry deposition on porous dolomitic limestones. Materials 3(1):216–231

Pinaev VA (1964) Mutual solubility of magnesium sulphite, bisulfite and sulfate. Zhirnal Prikladnoi Khimii 37:1361–1362

Przepiórski J, Czyzewski A, Kapica J, Moszynski J, Grzmil B, Tryba B, Mozia S, Morawski AW (2012) Low temperature removal of SO_2 traces from air by MgO-loaded porous carbons. Chem Eng J 191:147–153

Rodríguez-Navarro C, Sebastián E (1996) Role of particulate matter from vehicle exhaust on porous building stones (limestone) sulfation. Sci Total Environ 187:79–91

Rowland CH, Abdulsattar AH (1978) Equilibriums for magnesia wet scrubbing of gases containing sulfur dioxide. Environ Sci Technol 12:1158–1162

Saiz-Jimenez C, Brimblecombe P, Camuffo D, Lefevre RA, Van Grieken R (2004) Damages caused to European monuments by air pollution: assessment and preventive measures. In: Saiz-Jimenez (ed) Air Pollution and cultural heritage. London, pp 91–109

Santamarina M, Di Cuarto F, Zanna S, Marcus P (2007) Initial surface film on photocurrent spectroscopy (PCS). Electrochim Acta 53:1314–1324

Schögg K, Steind M, Friedl A, Weber HK, Sixta H (2006) Calculation of physical property data of the system $MgO–SO_2–H_2O$ and their implementation in Aspen Plus®. Lenzinger Berichte 86:56–62

Seinfeld JH, Pandis SN (1998) Atmospheric chemistry and physics: from air pollution to climate change. Wiley, New York

Söhnel O, Rieger A (1994) Solubilities of magnesium sulfite hydrates. J Chem Eng Data 39:161–162

Tambe S, Gauri KL, Li S, Cobourn WG (1991) Kinetic study of the SO_2 reaction with dolomite. Environ Sci Technol 25:2071–2075

Tommervik H, Johansen BE, Pedersen JP (1995) Monitoring vegetation changes in Pasvik (Norway) and Pechenga in Kola Peninsula (Russia) using multitemporal Landsat MSS/TM data. Sci Total Environ 160(161):753–767

Török A (2002) Oolitic limestone in polluted atmospheric environment in Budapest weathering phenomena and alterations in physical properties. In: Siegesmund S, Weiss T, Vollbrecht A (eds) Natural stone, weathering phenomena, conservation strategies and case studies. Special Publications, vol 205. Geological Society, London, pp 363–379

Török A (2008) Black crusts on travertine: factors controlling development and stability. Environ Geol 56:583–594

Török A, Licha T, Simon K, Siegesmund S (2011) Urban and rural limestone weathering: the contribution of dust to black crust formation. Environ Earth Sci 63:675–693

Torrisi A (2008) XPS study of five fluorinated compounds deposited on calcarenite stone: Part I. Unaged samples. Appl Surf Sci 254:2650–2658

Viles HA (1990) The early stages of building stone decay in an urban environment. Atmos Environ 24A:229–232

Winkler EM (1966) Important agents of weathering for building and monumental stone. Eng Geol 1:381–400